Supporting Information

Rapid and green Etching of MAX into MXene Phase Via physical process

Feng Gao,[a] Junqi Liu,[a] Xiaohua Qiao,[a] Qilin Zheng,[a] Ruifeng Qi[†a] and Qingsong Huang[*ab]

[a.] School of Chemical Engineering, Sichuan University, Chengdu 610065, China. *Corresponding author 1. E-mail: qshuang@scu.edu.cn. † Corresponding author 2. E-mail: qrf602459322@163.com.
[b.] Tianfu Jiangxi Laboratory, Chengdu 610065, China.

Table S1 Comparison of the etching time in this work with those reported in the literature for MXene.

Type of material	Etchant	Time	Reference
V_2AlC	**$CuCl_2$**	**4 min**	**This work**
Ti_3SiC_2	$CuCl_2$	24 h	Ref. [1]
V_2AlC	$NiCl_2$	24 h	Ref. [2]
V_2AlC	$CuCl_2$	10 h	Ref. [3]
Ti_3AlC_2	$FeCl_2$	24 h	Ref. [4]
Nb_2AlC	SnF_2	6-36 h	Ref. [5]
Ti_3AlC_2	$CoCl_2$	24 h	Ref. [6]
V_2AlC	HF and HCl	72 h	Ref. [7]

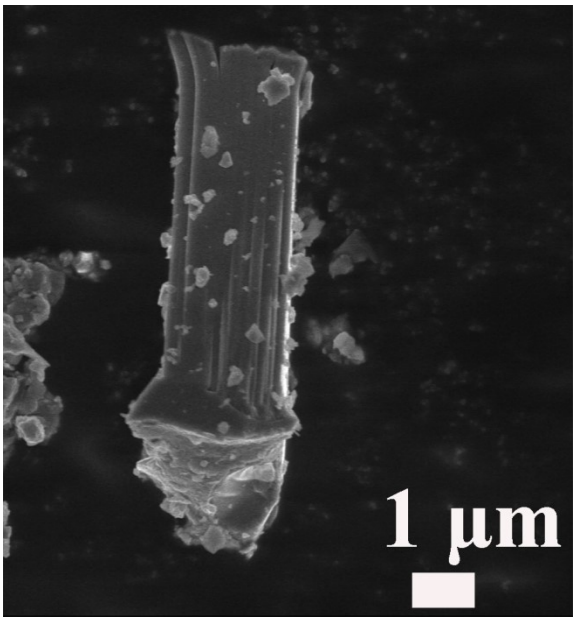

Figure S1. Scanning electron microscopy (SEM) image of the V_2AlC.

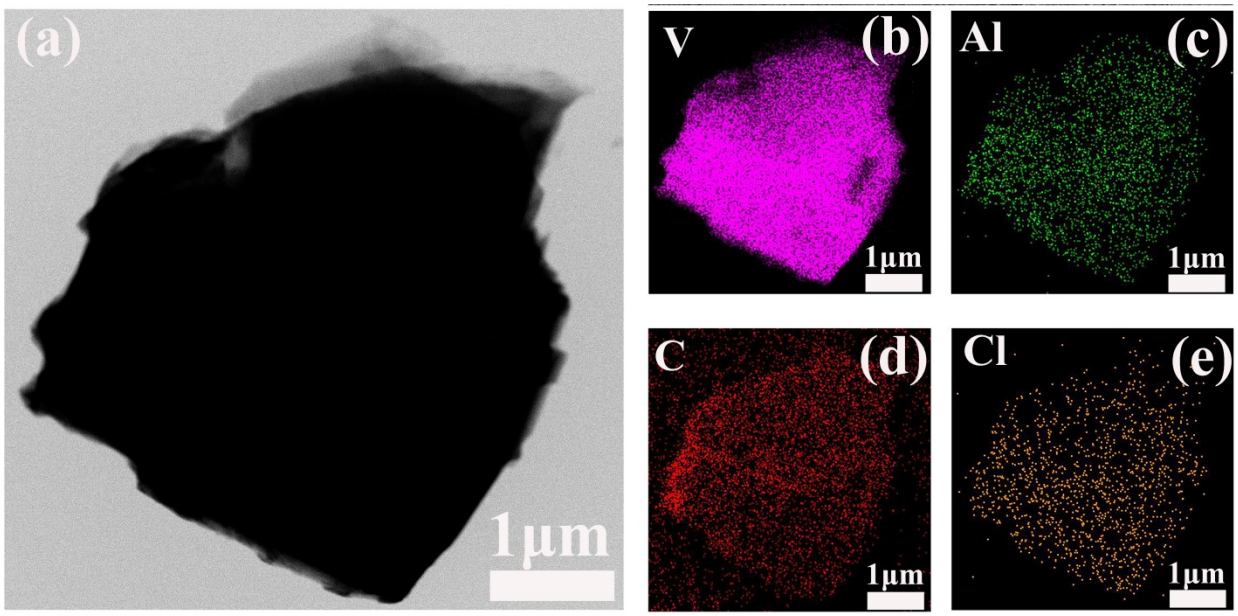

Figure S2. (a-e) EDS mapping images of the AA-240 sample. Purple, green, red, and orange represent V, Al, C, and Cl, respectively.

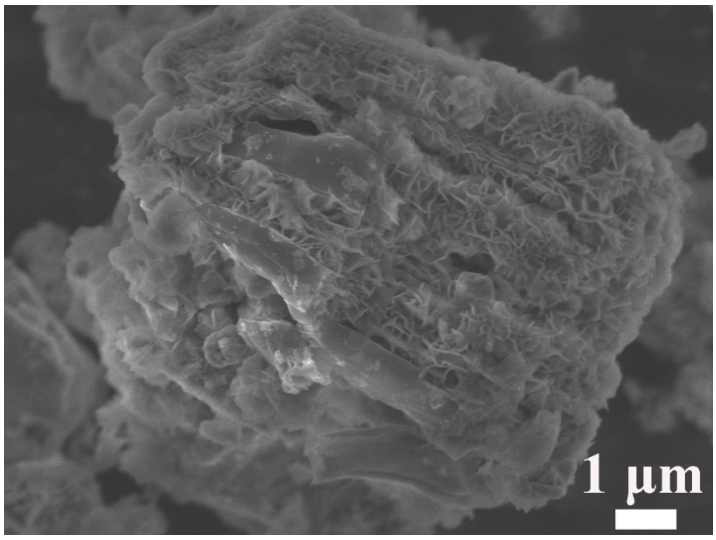

Figure S3. The SEM image after continuous etching for 240 s showed a fish-scale-like structure.

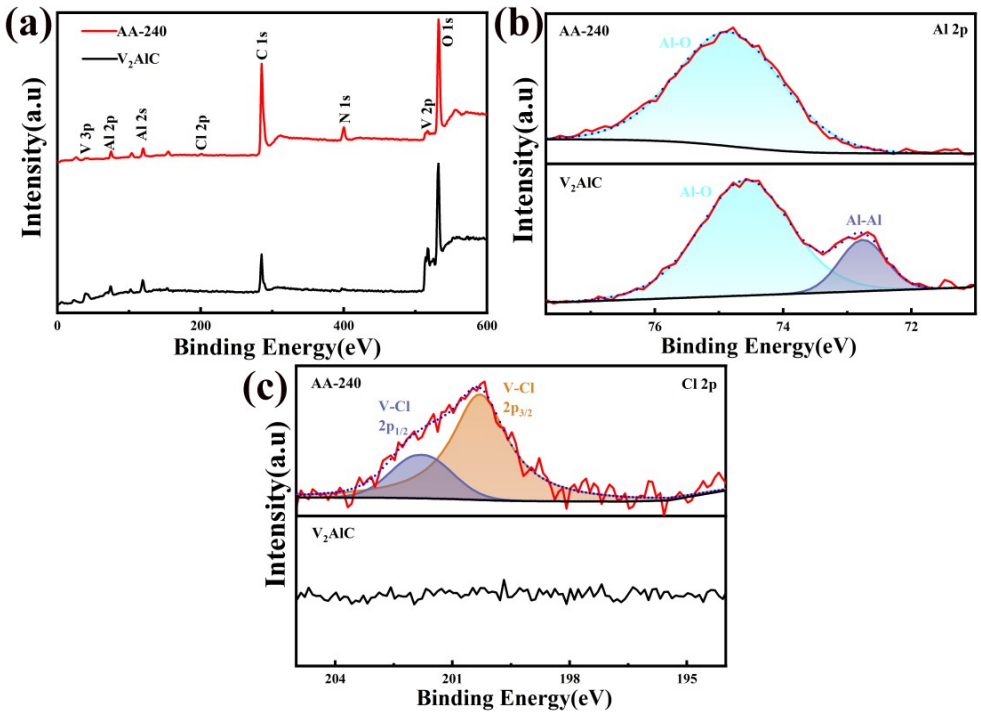

Figure S4. XPS spectra of the AA-240 sample (a) XPS survey spectrum. (b) Al 2p high-resolution spectra. (C) Cl 2p high-resolution spectra.

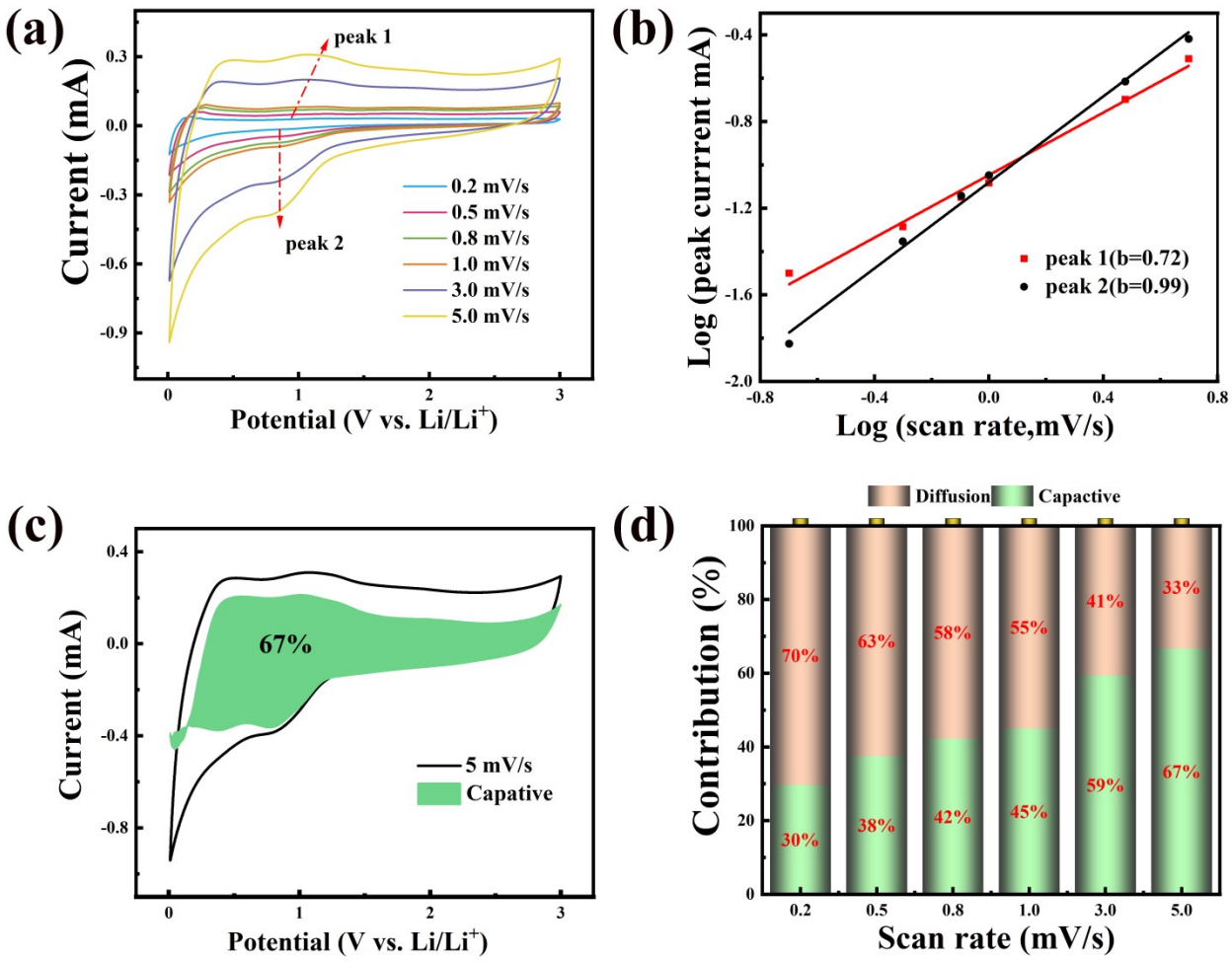

Figure S5. Lithium storage kinetics of the AA-240 sample: (a) CV curves of the AA-240 sample at different scan rates. (b) Log(i)–log(v) plot of the AA-240 sample for determining the b-value. (c) Capacitive contribution curve (shaded region) of the AA-240 sample at 5 mV s^{-1}. (d) Capacitive contribution ratio of the AA-240 sample at different scan rates. (see detail in the Electrochemical Measurement section)

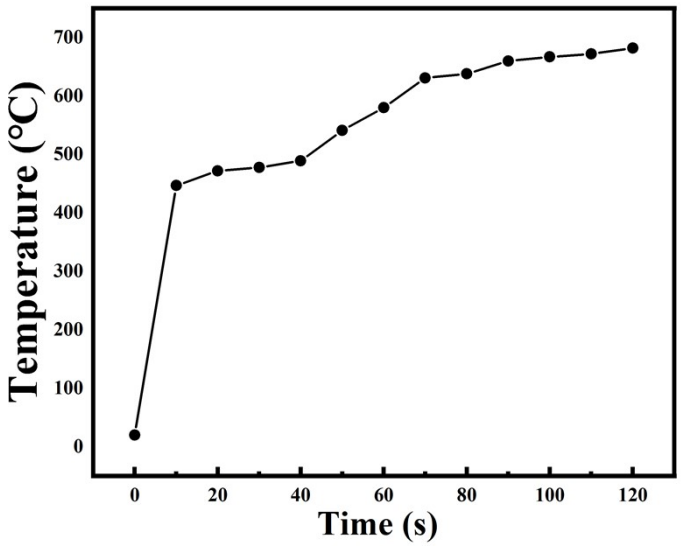

Figure S6. Temperature measurement of graphite paper under periodic intermittent heating mode at a current of 18.7 A. The temperature was recorded immediately after each 10-second heating phase (data were not collected during the cooling periods). Each data point represents the instantaneous temperature at the end of a heating phase.

Table S2 Lithium storage performance comparison of different MXenes.

Type of material	Etching Method	Current (mA g^{-1})	Cycle Number	Capacity (mAh g^{-1})	Reference
V_2C	**DMF-CMS**	**100**	**80**	**370**	**This work**
$Ti_3C_2(OH)_2$	KOH	100	250	143.4	Ref. [8]
Ti_2CT_x	HF	100	525	140	Ref. [9]
s-Ti_2CT_x	LiF and HCl	1500	1000	148	Ref. [10]
V_2C	CVD	100	500	385.2	Ref. [11]
Oxidized V_2CT_x	HF, H_2O_2	100	100	318	Ref. [12]
Nb_2CT_x	Lewis acidic	50	50	330	Ref. [13]
LS-Mo_2CT_x	HF	1000	1000	340	Ref. [14]

Materials and methods

Synthesis of V_2AlC: Combine V (Baima, Tianjin, China, 99.99 wt.%, -400 mesh), Al (Chengdu, China, 99 wt.%, -325 mesh), and C (Alanding Industrial Co., Ltd., China, 99.95 wt.%, -325 mesh) were mixed in a 2:1.2:1 molar ratio. The mixture was vacuum-ground in a ball mill at 500 r/min for 45 minutes. A non-stoichiometric ratio was chosen to compensate for Al volatilization at high temperatures. Subsequently, 2.0 g of the mixed powder was pressed into cylindrical blocks with a diameter of 20 mm using a hydraulic press. The pressed blocks were placed in an alumina crucible and heated in a magnetically levitated melting furnace, which had been purged three times with argon gas, using graphite paper as the heat source. After heating for 80 seconds at 5 kPa (absolute pressure) and 25.0 A, argon gas was immediately introduced

as a protective atmosphere while restoring atmospheric pressure. The sample was cooled for 8 minutes to obtain a compacted specimen. Finally, the specimen was manually ground into powder and collected by sieving through a 500-mesh screen.

Synthesis of V_2C MXene: 0.174 g of V2AlC synthesized by the aforementioned method, 0.497 g of CuCl2, 0.144 g of NaCl, and 0.186 g of KCl were weighed in a molar ratio of 1:3:2:2. The materials were ground and mixed thoroughly, then pressed into cylindrical blocks with a diameter of 20 mm using a hydraulic press. The pressed blocks were placed in an alumina crucible and loaded into a magnetic levitation furnace that had been purged three times with argon gas. Heating was performed using graphite paper as the heating element. The heating conditions were 5 kPa (absolute pressure) and 18.7 A current, employing a periodic intermittent heating mode: each cycle comprised 10 seconds of heating followed by 10 seconds of cooling. This cycle was repeated to achieve cumulative reaction times of 60, 120, 180, and 240 seconds. For the two etching experiments, after accumulating 120 seconds under the cyclic intermittent heating mode, the sample was cooled to room temperature and subjected to an additional identical heating cycle, resulting in a cumulative reaction time of 240 seconds (Figure S6). Following reaction completion, the product was washed with deionized water to remove residual salts, yielding MXene/Cu composite particles. Subsequently, the composite was treated with a 0.2 M/L ammonium persulfate (APS) solution to eliminate residual Cu particles. The treated suspension underwent three alternating washes with deionized water and ethanol, followed by filtration through a 0.45 μm microporous membrane. Finally, the collected solid product was vacuum-dried at 80 ℃ for 12 hours to obtain the target powder samples. Samples etched once using the DMF-CMS method were designated A-X, where X represents the total time after several cycles, including the heating and cooling time within each cycle. Samples etched twice using the DMF-CMS method were designated AA-X, where X represents the total time after several cycles, including the heating and cooling time within each cycle.

Materials characterization and electrochemical measurement

Characterization of the samples: Phase identification and crystal structure refinement were performed using XRD (Bruker D8 ADVANCE A25X with Cu Kα radiation). Data was collected over a 2θ range from 5 ° to 80 ° with a step size of 0.02 ° and a dwell time of 2 s. The XRD patterns of all samples were obtained under the same testing conditions. The morphology of the collected samples was characterized by field emission scanning electron microscopy (ZEISS Sigma 300, Germany). The sample for transmission electron microscopy (TEM) analysis was prepared by diluting powder in alcohol, subjecting it to ultrasonic treatment, and then dispersing it onto a copper grid. The surface morphology and lattice structure of V_2C was characterized using high-resolution transmission electron microscopy (HRTEM, JEOL, Japan) at an accelerating voltage of 200 kV. Elemental mapping and local composition were analyzed via energy-dispersive X-ray spectroscopy (EDS) using a JEOL JED-2200 detector. X-ray photoelectron spectroscopy (XPS) data was acquired using a Thermo Scientific K-Alpha spectrometer equipped with an Al Kα X-ray source (hv = 1486.6 eV).

Electrochemical Measurement: The active material V_2C, conductive carbon black, and polyvinylidene fluoride (PVDF) were uniformly mixed in a mass ratio of 7:2:1. N-methyl-2-pyrrolidone (NMP) solvent was added, and the mixture was stirred to form a homogeneous slurry. Subsequently, the slurry was coated onto a copper foil and vacuum-dried at 80 °C for 24 hours to obtain the working electrode, which was then cut into circular discs with a diameter of 12 mm using a disc cutter. CR2032-type coin cells were assembled in an argon-filled glove box (with water and oxygen content both below 1 ppm), using lithium metal foil as the counter electrode and Celgard 2325 as the separator. The electrolyte was a 1 M LiPF6 solution in EC/DEC/DMC (volume ratio 1:1:1). After assembly, the batteries were left to stabilize for 12 hours. Galvanostatic charge-discharge (GCD) tests were then performed within a voltage range of 0.01-3.0 V (vs. Li/Li^+) using a Neware battery testing system. Cyclic voltammetry (CV) tests were conducted within the same voltage range (0.01-3.0 V (vs. Li/Li^+)) using a CHI 760E electrochemical workstation. To quantitatively analyze the charge storage kinetics of the V_2C electrode, the functional relationship between the peak current (***i***) and the scan rate (***v***) was studied via cyclic voltammetry. This relationship can be expressed by Equation (1):

$$\boldsymbol{i} = a\boldsymbol{v}^b \tag{1}$$

where a and b are fitting parameters. Taking the logarithm of Equation (1) yields the linear relationship:

$$\log(\boldsymbol{i}) = b\log(\boldsymbol{v}) + \log(a) \tag{2}$$

The parameter b can be obtained by fitting the slope of the log(***i***) versus log(***v***) curve. This parameter can be used to determine the dominant charge storage mechanism: when b ≈ 0.5, it indicates a process mainly controlled by ion diffusion; when b ≈ 1.0, it indicates surface-controlled pseudocapacitive behavior is dominant. The contributions of capacitive and diffusion processes to the total charge storage can be further quantified using Equation (3), where i, k_1v,

and $k_2v^{1/2}$ represent the total current, the capacitance-controlled current, and the diffusion-controlled current, respectively.

$$\boldsymbol{i} = k_1v + k_2\boldsymbol{v}^{1/2} \quad (3)$$

References:

1 Y. Li, H. Shao, Z. Lin, J. Lu, L. Liu, B. Duployer, P. O. Å. Persson, P. Eklund, L. Hultman, M. Li, K. Chen, X.-H. Zha, S. Du, P. Rozier, Z. Chai, E. Raymundo-Piñero, P.-L. Taberna, P. Simon and Q. Huang, *Nat*. *Mater*., 2020, **19**, 894–899.
2 Y. Wang, W. Lv, G. Wu, W. Zhang and Z. Li, *Appl Surf Sci*, 2023, **637**, 157911.
3 R. Nittoor-Veedu, B. Kalleshappa and M. Pumera, *ACS Nano*, 2025, **19**, 39645–39653.
4 P. Huang, H. Ying, S. Zhang, Z. Zhang and W. Han, *Adv Energy Mater*, 2022, **12**, 2202052.
5 K. Arole, J. W. Blivin, A. M. Bruce, S. Athavale, I. J. Echols, H. Cao, Z. Tan, M. Radovic, J. L. Lutkenhaus and M. J. Green, *Chem*. *Commun*., 2022, **58**, 10202–10205.
6 Z. Wang, F. Dong, L. Tan, S. Xiong and J. Feng, *Nano Let*t, 2025, **25**, 17308–17316.
7 Q. Zhang, H. Wang, X. Kong, Y. Wu, Y. Mao, M. Jiao, R. Lian, Y. Fang, W. Liu, J. Wang, Z. Zhou, D. Cao and K. Zhu, *Adv Energy Mater*, 2026, **16**, e04697.
8 B. Zhang, J. Zhu, P. Shi, W. Wu and F. Wang, *Ceram Int*, 2019, **45**, 8395–8405.
9 C. Wu, R. Qi, X. Zhang, Q. Liu and Q. Huang, *Chem. Commun*., 2019, **55**, 7522–7525.
10 C. Cui, R. Dai, C. Zhang, B. Fan and X. Wang, *J. Mater. Chem. A*, 2022, **10**, 15474–15484.
11 W. Ding, D. Cakir, L. R. Jaishi, J. Yuan, M. Anas, P. Kharel, B. Yao and X. Xian, *J. Mater. Chem. A*, 2026, 10.1039/D5TA09038E.
12 W. Luo, Y. Liu, F. Li, J. Huo, D. Zhao, J. Zhu and S. Guo, *Appl Surf Sci*, 2020, **523**, 146387.
13 H. Dong, P. Xiao, N. Jin, B. Wang, Y. Liu and Z. Lin, *ChemElectroChem*, 2021, **8**, 957–962.
14 Z. Bayhan, J. K. El-Demellawi, J. Yin, Y. Khan, Y. Lei, E. Alhajji, Q. Wang, M. N. Hedhili and H. N. Alshareef, *Small*, 2023, **19**, 2208253.